

AD-A213 792

DTIC FILE COPY

ESL-TR-87-22

1

ROCK MODELING USING THE CENTRIFUGE

P.G. JOSEPH, H.H. EINSTEIN

MASSACHUSETTS INSTITUTE OF TECHNOLOGY
DEPARTMENT OF CIVIL ENGINEERING
CAMBRIDGE, MASSACHUSETTS 02139

JUNE 1988

FINAL REPORT

APRIL 1986 - DECEMBER 1986

DTIC
ELECTE
OCT 30 1989
S D

APPROVED FOR PUBLIC RELEASE: DISTRIBUTION UNLIMITED



AFESC

ENGINEERING & SERVICES LABORATORY
AIR FORCE ENGINEERING & SERVICES CENTER
TYNDALL AIR FORCE BASE, FLORIDA 32403

89 10 27 179

NOTICE

PLEASE DO NOT REQUEST COPIES OF THIS REPORT FROM
HQ AFESC/RD (ENGINEERING AND SERVICES LABORATORY).
ADDITIONAL COPIES MAY BE PURCHASED FROM:

NATIONAL TECHNICAL INFORMATION SERVICE
5285 PORT ROYAL ROAD
SPRINGFIELD, VIRGINIA 22161

FEDERAL GOVERNMENT AGENCIES AND THEIR CONTRACTORS
REGISTERED WITH DEFENSE TECHNICAL INFORMATION CENTER
SHOULD DIRECT REQUESTS FOR COPIES OF THIS REPORT TO:

DEFENSE TECHNICAL INFORMATION CENTER
CAMERON STATION
ALEXANDRIA, VIRGINIA 22314

REPORT DOCUMENTATION PAGE				Form Approved OMB No. 0704-0188		
1a. REPORT SECURITY CLASSIFICATION UNCLASSIFIED			1b. RESTRICTIVE MARKINGS			
2a. SECURITY CLASSIFICATION AUTHORITY			3. DISTRIBUTION / AVAILABILITY OF REPORT			
2b. DECLASSIFICATION / DOWNGRADING SCHEDULE			Approved for public release. Distribution unlimited.			
4. PERFORMING ORGANIZATION REPORT NUMBER(S)			5. MONITORING ORGANIZATION REPORT NUMBER(S)			
			ESL-TR-87-22			
6a. NAME OF PERFORMING ORGANIZATION Massachusetts Institute of Technology		6b. OFFICE SYMBOL (if applicable)	7a. NAME OF MONITORING ORGANIZATION Air Force Engineering and Services Center			
6c. ADDRESS (City, State, and ZIP Code) Department of Civil Engineering Cambridge, Massachusetts 02139			7b. ADDRESS (City, State, and ZIP Code) HQ AFESC/RDCS Tyndall Air Force Base, Florida 32403-6001			
8a. NAME OF FUNDING / SPONSORING ORGANIZATION		8b. OFFICE SYMBOL (if applicable)	9. PROCUREMENT INSTRUMENT IDENTIFICATION NUMBER Contract #DACA88-86-D-0013			
8c. ADDRESS (City, State, and ZIP Code)			10. SOURCE OF FUNDING NUMBERS			
			PROGRAM ELEMENT NO. 6.2	PROJECT NO. 2673	TASK NO. 0074	WORK UNIT ACCESSION NO. N/A
11. TITLE (Include Security Classification) Rock Modeling Using the Centrifuge						
12. PERSONAL AUTHOR(S) P. G. Joseph, H. H. Einstein						
13a. TYPE OF REPORT Final		13b. TIME COVERED FROM Apr 86 to Dec 86		14. DATE OF REPORT (Year, Month, Day) June 1988		
15. PAGE COUNT 56						
16. SUPPLEMENTARY NOTATION Availability of this report is specified on reverse of front cover.						
17. COSATI CODES			18. SUBJECT TERMS (Continue on reverse if necessary and identify by block number)			
FIELD	GROUP	SUB-GROUP				
			Rock Mechanics Centrifuge Modeling			
			Scaling Relationships Small-Scale Modeling			
19. ABSTRACT (Continue on reverse if necessary and identify by block number) This report investigates the use of the centrifuge for studying various topics in rock mechanics. The report has three chapters. The first chapter deals with scaling relations developed specifically for rock and establishes requirements that must be satisfied for model-prototype similitude. The second chapter details various areas in rock mechanics which can be profitably investigated using the centrifuge. In the third chapter, tests that will provide information on these areas will be proposed and any problems likely to be encountered will be examined.						
20. DISTRIBUTION / AVAILABILITY OF ABSTRACT <input checked="" type="checkbox"/> UNCLASSIFIED/UNLIMITED <input type="checkbox"/> SAME AS RPT. <input type="checkbox"/> DTIC USERS			21. ABSTRACT SECURITY CLASSIFICATION UNCLASSIFIED			
22a. NAME OF RESPONSIBLE INDIVIDUAL STEVEN T. KUENNEN, 2Lt, USAF			22b. TELEPHONE (Include Area Code) (904) 283-6298		22c. OFFICE SYMBOL HQ AFESC/RDCS	

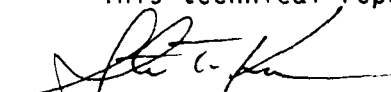
PREFACE


This report was submitted as a dissertation to Massachusetts Institute of Technology funded under Job Order Number 26730074 by the Air Force Engineering and Services Center, Engineering and Services Laboratory, Tyndall AFB, Florida 32403-6001.

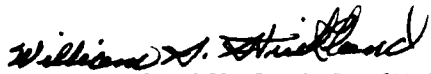
This dissertation is being published in its original format by this laboratory because of its interest to the worldwide scientific and engineering community. This dissertation covers work performed between April 1986 and December 1986. AFESC/RD project officers were Paul L. Rosengren, Jr., and 1Lt Steven T. Kuennen.

This report has been reviewed by the Public Affairs Officer (PA) and is releasable to the National Technical Information Service (NTIS). At NTIS, it will be available to the general public, including foreign nationals.

This technical report has been reviewed and is approved for publication.


STEVEN T. KUENNEN, 2Lt, USAF
Project Officer


ROBERT J. MAJKA, Lt Col, USAF
Chief, Engineering Research Division


WILLIAM S. STRICKLAND, GM-14
Chief, Facility Systems and
Analysis Branch


JAMES R. VAN ORMAN
Deputy Director of Engineering
and Services Laboratory

Table of Contents

		Page Number
Chapter 1	Scaling Relations	1
1.1	Introduction	1
1.2	Scaling relations for intact rock	1
1.3	Scaling relations for a joint surface	13
1.4	Conclusion	33
Chapter 2	Proposed Rock Mechanics Research Using the Centrifuge	35
2.1	Introduction	35
2.2	Proposed research	35
2.3	Problems involved with centrifuge tests of rock	41
Chapter 3	The Testing Program	43
3.1	Introduction	43
3.2	The testing program	43
3.3	Conclusion	49
References		50



Accession for	
NTIS - CRA&	<input checked="" type="checkbox"/>
DTIC TAB	<input type="checkbox"/>
Unannounced	<input type="checkbox"/>
By _____	
DTIC TAB	
Availability Codes	
Dist	Availability Codes
A-1	

Chapter 1. Scaling Relations

1.1 Introduction

Small scale models are a relatively inexpensive and convenient way of studying prototype behavior. For similitude between model and prototype, the model has to be scaled so as to satisfy certain requirements. These requirements are the scaling relations between the model and prototype and, as explained in the accompanying report, can be obtained using the governing equation of the phenomena being modelled or by using dimensional analysis. This chapter examines the scaling relations applicable for intact rock and for a joint surface.

1.2 Scaling relations for intact rock

The problem of modelling intact rock in an elevated g-field such as that produced in a centrifuge was studied by Hoek (1965). The intact rock was modelled as an elastic body in thermal equilibrium. His approach was as follows:

The behavior of a point in the structure, defined by co-ordinates x , y and z , depends on the geometry of the structure, the material properties and the applied stresses. Consequently for the behavior of the corresponding point in the model to be the same as that in the prototype, similitude between the model and prototype has to be established regarding the geometry, the material properties and the applied stresses. To do this, the prototype must first be described in terms of its geometry, material properties and, the stresses, accelerations etc. imposed on it. First the geometry of the structure will be considered.

Let the geometry of the prototype structure be defined as

L = a typical length dimension for example the diameter of a tunnel opening

r^L = a set of dimensionless ratios relating other length dimensions of the structure to L .

The geometry of the prototype is now defined.

Let the material properties of the prototype at this point (x, y, z) be defined as

ρ = the density of the material.

E = the Young's modulus of the material.

ν = the Poisson's ratio of the material.

There may be more than one material present in the structure, or the properties may depend on the state of stress at that point. Consequently, the material properties at various points in the structure need not be the same as those at points x, y, z . If this is the case, then let the properties at the various points be related to the properties at point x, y, z by the set of dimensionless ratios r^ρ, r^E and r^ν . The material properties of the prototype and their distribution within the prototype are now described.

The remaining area where a description of the prototype is required is in the mechanically applied stresses, forces, etc. The stresses imposed on the model consist of both external and internal stresses. Tectonic stress or a stress due to gravitational body forces are examples of internal stresses. Let the applied loads, stresses, displacement and accelerations at point (x, y, z) be

Q = an externally applied load

P = an externally applied stress

σ_o = an internal stress

g = acceleration which the entire body is subject to, and which results in self-weight body forces.

U_o = a displacement imposed directly on only a part of the structure.

γ = an acceleration imposed directly only on part of the structure.

The applied loads, stresses, displacements and accelerations at other points may not be the same as those at point x, y, z . In this case let them be related to those at the point x, y, z , by a set of dimensionless ratios $r_Q, r_P, r_{\sigma o}, r_{U_o}, r_\gamma$.

Now the resulting displacement ' u ' or the resulting stress ' σ ' at point x, y, z is some function of the above variables.

Thus,

$$u = f(x, y, z, t, L, \rho, E, Q, P, \sigma_o, g, v, \nu, r^L, \dots r^\nu) \quad (1)$$

and

$$\sigma = f(x, y, z, t, L, \rho, E, Q, P, \sigma_o, g, v, \nu, r^L, \dots r^\nu) \quad (2)$$

As shown in the accompanying report [Joseph et al (1987)], by using dimensional analysis, the above variables can be rearranged to form the following dimensionless products.

$$\frac{u}{L}, \frac{\sigma L^2}{Q}, \frac{x}{L}, \frac{y}{L}, \frac{z}{L}, \frac{t\gamma^{1/2}}{L^{1/2}}, \frac{EL^2}{Q}, \frac{\rho\gamma L^3}{Q}, \frac{g}{\gamma}, \frac{PL^2}{Q}, \frac{U_o}{L}, \frac{\sigma_o L^2}{Q} \text{ and } \nu$$

Buckingham's Theorem (also called the Π theorem) states that if an equation is homogenous, it can be reduced to a relationship among a complete set of dimensionless products. In other words, displacement u or stress σ , in the form of a dimensionless product, can be related to all other variables when expressed as a complete set of dimensionless products. Using the complete set just obtained, the following equations result.

$$\frac{u}{L} = F \left[\frac{x}{L}, \frac{y}{z}, \frac{z}{L}, \frac{t\gamma^{1/2}}{L^{1/2}}, \frac{EL^2}{Q}, \frac{\rho\gamma L^3}{Q}, \frac{g}{\gamma}, \frac{PL^2}{Q}, \frac{U_o}{L}, \frac{\sigma_o L^2}{Q} \right]$$

$$v, r^L, r^E, r^v, r^Q, r^P, r^{U_o}, r^\rho, r^{\sigma_o}, r^\gamma] \quad (3)$$

$$\text{and } \frac{\sigma_o L^2}{Q} = F' \left[\frac{x}{L}, \dots, r^\gamma \right] \quad (4)$$

where F and F' are functions expressing the relations among the dimensionless terms. These dimensional products provide a means of ensuring that model behavior simulates prototype behavior. For complete similarity between model and prototype, the dimensionless products of the model should be the same as the corresponding products of the prototype. In other words, for complete similitude between model and prototype,

$$\Pi_{i_{\text{Model}}} = \Pi_{i_{\text{Prototype}}}, \text{ for all } i\text{'s.}$$

From equations (3) and (4), one can see that similitude between model and prototype requires that the similitude requirements with regard to geometry, material properties and applied stresses, displacements, accelerations and forces be satisfied. Equality of the terms $\frac{x}{L}$, $\frac{y}{L}$, $\frac{z}{L}$ means that the same point in the model is being considered. Equality of the ratios r^L ensures strict geometric similitude between model and prototype. In order that similitude with respect to material properties be satisfied at a particular point, the dimensionless products that contain in them any of the material properties, should be the same in both the model and the prototype (at this point). The dimensionless terms involving the material properties are

$$\nu, \frac{\rho \gamma L^3}{Q}, \text{ and } \frac{Q}{EL^2}$$

One of the advantages of dimensionless products is that similitude between model and prototype requires that the values of only the dimensionless products be equal in both model and prototype, while the values of the individual terms that make up the product need not be equal. For example, consider the dimensionless product $\frac{EL^2}{Q}$, and let the suffix m and p refer to

the model and the prototype respectively. As long as $\frac{E_m L_m^2}{Q_m^2} = \frac{E_p L_p^2}{Q_p^2}$

it is not important if E_m is not equal to E_p i.e. differences between E_m and E_p can be compensated for by suitably adjusting the values of L and Q , such that the value of the complete dimensional product is the same in both the model and the prototype. The Poisson's ratio ν is dimensionless by itself and consequently cannot be included meaningfully as part of any dimensionless product. This means that, the Poisson's ratio should be the same in both the model and the prototype or, that

$$\nu_m = \nu_p \quad (5)$$

Often, model materials, that satisfy various other requirements do not have the same Poisson's ratio as the prototype material. For some problems, the effect of Poisson's ratio on the stress distribution is small, while for other problems, the effect is significant, in which case, a suitable correction can be made. The main effect of the Poisson's ratio is in the lateral stresses induced in a body whose lateral deformation is restricted. The relationship between the applied vertical and the induced lateral stresses is given by

$$\sigma_1 = \frac{\nu}{1-\nu} \sigma_v \quad (6)$$

where, σ_1 is the induced lateral stress

σ_v is the applied vertical stress and

ν is the Poisson's ratio of the material.

Changes in the Poisson's ratio result in large changes in the lateral stresses and a correction should be made to the resulting stress field using the above equation. Hoek (1965) suggested an experimental procedure in which the model is placed on a liquid filled rubber bag. The model is free to deform laterally and the stress field is uniaxial. To bring the lateral stresses to their correct value, bags filled with a liquid of the correct density are placed on the sides of the model as shown in Fig. 1. Practically, however, it will be difficult to find rubber bags that can withstand the high stresses involved. If the bags can handle the stresses involved, then the technique will be of use when stress freezing photoelastic models. During stress freezing, the photoelastic material has a Poisson's ratio approaching 0.5 which is quite different from most rocks and consequently a correction (such as the one just described) should be applied to maintain similitude of the lateral stresses.

Another advantage of dimensionless products is that they can be multiplied among themselves to form other dimensionless products. Thus the dimensionless products containing ρ and E namely

$$\frac{\rho \gamma L^3}{Q} \text{ and } \frac{Q}{EL^2} \text{ can be combined as}$$

$$\frac{\rho \gamma L^3}{Q} \cdot \frac{g}{\gamma} \cdot \frac{Q}{EL^2} = \frac{\rho g L}{E}$$

to form another dimensionless product i.e. $\frac{\rho g L}{E}$ that contains both the remaining material properties ρ and E .

$$\text{Hence, if } \frac{\rho_m g_m L_m}{E_m} = \frac{\rho_p g_p L_p}{E_p} \text{ or if}$$

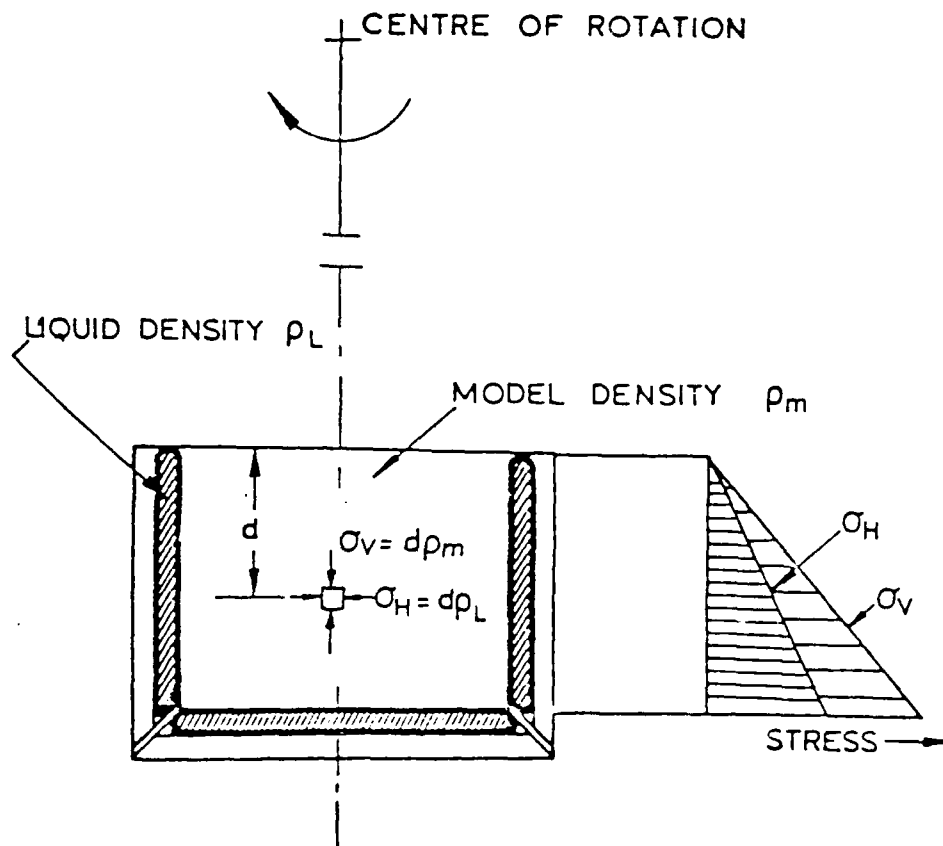


Fig. 1. Experimental correction to account for different Poisson's ratio in model and prototype. From Hoek (1965).

$$\frac{L_p}{L_m} = \frac{E_p}{E_m} \cdot \frac{\rho_m}{\rho_p} \cdot \frac{g_m}{g_p} \quad (7)$$

then material similitude between the two points is obtained. If, in addition, the ratios $r\rho$, rE and rg are the same in both model and prototype, then material similitude is ensured between the entire model and prototype. Sometimes, however, the resulting model stresses and displacements σ_m and u_m may not be suited to the measuring capabilities of the instrument in which case, as suggested by Hoek (1965) they can be scaled by a factor, say α , such that

$$\sigma_p = \alpha \sigma_m \quad \text{and}$$

$$u_p = \alpha u_m$$

This can be obtained by altering the material properties alone such that

$$\frac{\alpha \rho_m g_m L_m}{E_m} = \frac{\rho_p g_p L_p}{E_p}$$

Hence equation (7) now becomes

$$\frac{L_p}{L_m} = \alpha \frac{E_p}{E_m} \frac{\rho_m}{\rho_p} \frac{g_m}{g_p} \quad (8)$$

Having ensured both geometric and material similitude, it remains to consider similitude in relation to the mechanically applied or induced stresses. These are defined by the parameters Q , P , σ_o , U_o and γ , and appear in the following dimensionless products:

$$\frac{t^2 \gamma}{L}, \quad \frac{EL^2}{Q}, \quad \frac{L^3 \rho \gamma}{Q}, \quad \frac{g}{\gamma}, \quad \frac{PL^2}{Q}, \quad \frac{U_o}{L} \quad \text{and} \quad \frac{\sigma_o L^2}{Q}$$

By suitably multiplying these terms, relations between the applied stresses in the model and prototype can be obtained in terms of the previously established relationships for the geometry and the material properties. The various relationships are as follows:

The relation between Q_m and Q_p can be determined in terms of the material and the geometry, using the dimensionless product $\frac{EL^2}{Q}$. Hence,

$$\frac{Q_m}{E_m L_m^2} = \frac{Q_p}{E_p L_p^2} \quad \text{or} \quad \frac{Q_m}{Q_p} = \frac{E_m}{E_p} \frac{L_m^2}{L_p^2} \quad (9)$$

The relation between P_m and P_p can be determined in terms of the material properties by defining a dimensionless product $\frac{P}{E}$

$$\frac{P}{E} = \frac{PL^2}{Q} \cdot \frac{Q}{EL^2}$$

$$\text{i.e.} \quad \frac{P_m}{E_m} = \frac{P_p}{E_p}, \quad \text{or} \quad \frac{P_m}{P_p} = \frac{E_m}{E_p} \quad (10)$$

Similarly the relation between σ_{o_m} and σ_{o_p} can be obtained in terms of the model material by defining the dimensionless product $\frac{\sigma_o}{E}$ given by

$$\frac{\sigma_o}{E} = \frac{\sigma_o L^2}{Q} \cdot \frac{Q}{EL^2}$$

$$\text{i.e.} \quad \frac{\sigma_{o_m}}{E_m} = \frac{\sigma_{o_p}}{E_p} \quad \text{or} \quad \frac{\sigma_{o_m}}{\sigma_{o_p}} = \frac{E_m}{E_p} \quad (11)$$

$$\text{Also,} \quad \frac{U_{o_m}}{L_m} = \frac{U_{o_p}}{L_p} \quad \text{or,} \quad \frac{U_{o_m}}{U_{o_p}} = \frac{L_m}{L_p} \quad (12)$$

The inertia forces are controlled by the dimensionless groups

$$\frac{\rho \gamma L^3}{Q} \quad \text{and} \quad \frac{\gamma}{g}$$

both of which have been used in obtaining equation (7) which controls the gravity forces in the model.

Since the inertia forces involve time, the scaling for time in terms of the material properties and the geometry, can be established by suitably

multiplying the dimensionless products to define the product $\frac{\rho L^2}{E t^2}$.

Hence

$$\begin{aligned} \frac{\rho L^2}{E t^2} &= \frac{\rho \gamma L^3}{Q} \cdot \frac{Q}{E L^2} \cdot \frac{L}{\gamma t^2} \\ \text{or} \quad \frac{\rho_m L_m^2}{E_m t_m^2} &= \frac{\rho_p L_p^2}{E_p t_p^2} \\ \text{i.e.} \quad \frac{t_m}{t_p} &= \left[\frac{E_p}{E_m} \frac{\rho_m}{\rho_p} \right]^{1/2} \frac{L_m}{L_p} \end{aligned} \quad (13)$$

If the scaling relations determined above are satisfied, then there will exist complete similitude between model and prototype.

Various investigators [Esser (1962) Haycocks (1962), Oudenhoven (1962), Hoek (1965)] used models made of photoelastic materials which they spun in the centrifuge. The isochromatic fringes obtained in these materials are proportional to the maximum shear stress τ_{\max} in the material. So, the greater the model shear stress, the better can the stress distribution in the model, and consequently in the prototype, be studied.

Let $\tau_{\max p} = \alpha \tau_{\max m}$

From equation (8), we get the q field that must be applied to the model to cause this shear stress as

$$\frac{q_m}{q_p} = \frac{1}{\alpha} \cdot \frac{L_p}{L_m} \cdot \frac{\rho_p}{\rho_m} \cdot \frac{E_m}{E_p} \quad (14)$$

As previously described, the Poisson's ratio should be the same in both model and prototype. For intact rock, the Poisson's ratio usually lies between 0.1 and 0.2 whereas for photoelastic materials, it approaches 0.5. Consequently, a correction of the type described earlier will have to be made to account for this error.

Hoek (1965) suggested that the centrifuge be used to study fracture and post failure behavior of rock, using model rock specimens. He assumed that the compressive strength was inversely proportional to the square root of the specimen size or

$$\sigma_{c_p} = \sigma_{c_m} \left(\frac{L_m}{L_p} \right)^{1/2} \quad (15)$$

where σ_{c_p} and σ_{c_m} are the stresses at failure in the model and prototype respectively, at failure. Consequently, if model stresses are a multiple of prototype stresses, we get

$$\begin{aligned} \sigma_{c_p} &= \alpha \left(\frac{L_m}{L_p} \right)^{1/2} \sigma_{c_m} \\ &= \beta \sigma_{c_m} \end{aligned} \quad (16)$$

and equation (8) now becomes

$$\begin{aligned}
 \frac{L_p}{L_m} &= \beta \frac{E_p}{E_m} \frac{\rho_m}{\rho_p} \frac{g_m}{g_p} \\
 &= \alpha \left(\frac{L_m}{L_p} \right)^{1/2} \frac{E_p}{E_m} \frac{\rho_m}{\rho_p} \frac{g_m}{g_p} \\
 \text{i.e. } \frac{g_m}{g_p} &= \frac{1}{\alpha} \left(\frac{L_p}{L_m} \right)^{3/2} \frac{E_m}{E_p} \frac{\rho_p}{\rho_m} \quad (17)
 \end{aligned}$$

which now accounts for the scaling of size with strength. It should be noted that equation (15) is based on the simplified assumption that crack length is proportional to size and that the bigger the specimen is, the larger will be the cracks and flaws that it will contain and consequently, the weaker it will be.

1.3 Scaling relations for a joint surface

1.3.1 Frictional joint behavior

In this section, the problem of modelling a joint on the centrifuge will be examined. Only joints with frictional behavior will be considered. Consequently, the problem reduces to modelling the frictional behavior between two sliding surfaces. There are two factors involved in this sliding process. One is the contact between the asperities and the other is the interlocking between the asperities.

Terzaghi (1920) and later Bowden and Tabor (1967) presented a theory for the frictional behavior related to asperity contacts. Large stresses at the asperities cause plastic flow in both brittle and ductile materials. As the normal load increases, the true area of solid to solid contact as shown in

Fig. 2, increases, so that the normal stress stays constant. During plastic flow, the shear stress is equal to the shear strength of the material. Consequently, since the solid to solid contact area increases, there is a proportional increase in the shear force required in order that the shear stress reaches its limiting value. In other words, the normal force and shear force are interdependent and related by the coefficient of friction $\mu = \tau/\sigma =$ a material constant.

Byerlee (1967) analysed a brittle material based purely on the theory of elasticity. He suggested that the tips of the asperities which are subject to both a normal force and a shear force, crush under the action of the normal force. The extent of crushing depends on the compressive strength of the material. When a shear force is applied, tensile stresses are induced in the asperities. If these induced tensile stresses exceed the local tensile strength, then additional breakage will take place. If all possible shapes of asperities are possible, then the shear and normal stresses are related as

$$\frac{\tau}{\sigma_n} = C_1 \frac{\sigma_t}{\sigma_c} + C_2$$

where, C_1 , C_2 = constants independent of the material

σ_t/σ_c = the ratio of the tensile strength to the compressive strength

The theories of Terzaghi (1920), Bowden and Tabor (1967) and Byerlee (1969) apply to that component of friction due to contact between the asperities. The second component governing frictional behavior between two surfaces is the interlocking between the asperities. Usually the two surfaces will not be in contact as shown in Fig. 2, with tip to tip contact between all

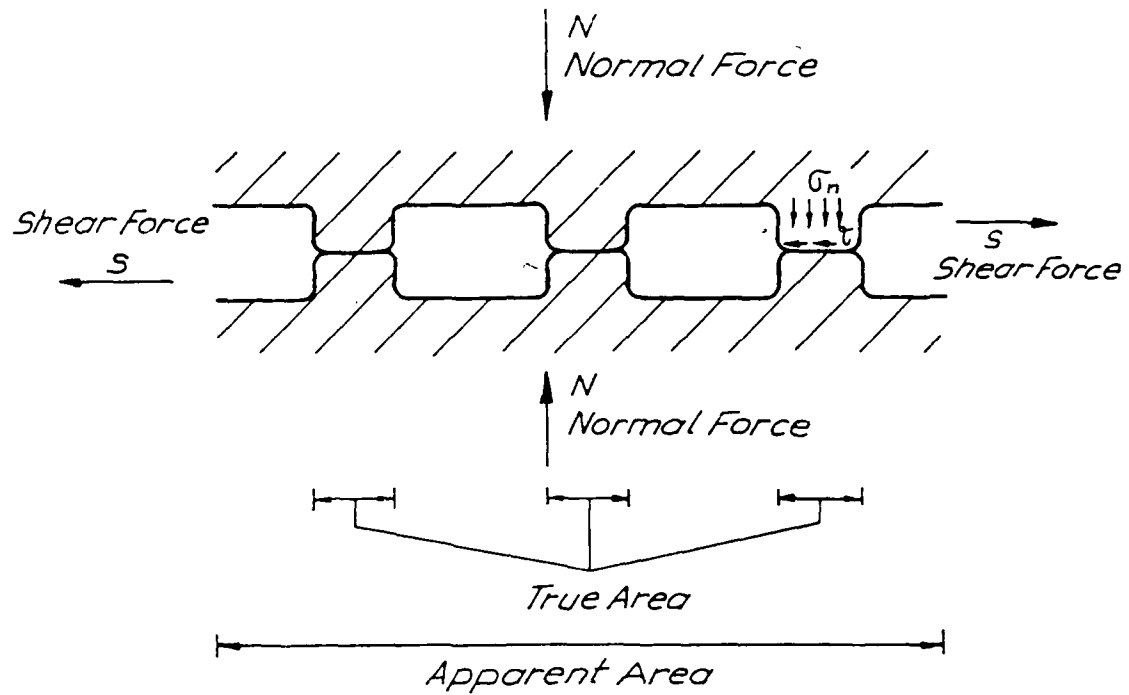


Fig. 2. Contact of Asperities. From Einstein et al (1970).

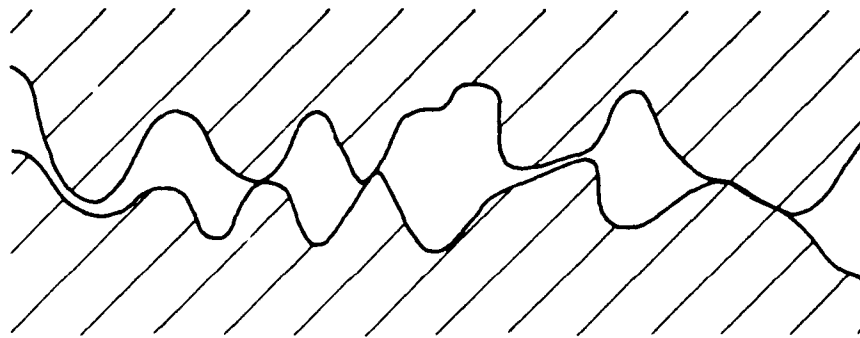


Fig. 3. Interlocking of asperities. From Einstein et al (1970).

the asperities. The real situation will be more like that shown in Fig. 3, in which only a few asperities will have tip to tip contact, while most will be staggered or interlocking. These interlocking asperities will influence the nature of the frictional behavior between the two surfaces. Einstein et al (1970) state that it is conceivable that the relative importance of the two mechanisms i.e. tip to tip contact between asperities and interlocking depends on the scale and nature of the surface. Consequently, friction due to tip to tip contact between the asperities will be of greater importance for smooth surfaces and on a microscopic scale, whereas for rough surfaces and on a macroscopic scale, the response will be governed primarily by interlocking. Fig. 4 shows the shearing behavior of a single idealized asperity. Under small to moderate normal stresses, the asperities will slide over each other as shown in Fig. 4b, resulting in dilatant behavior. During this phase, the shearing resistance is given by

$$S = N \tan (\phi_s + i)$$

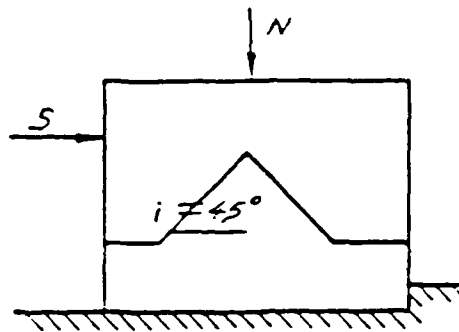
where S = shear force

N = normal force

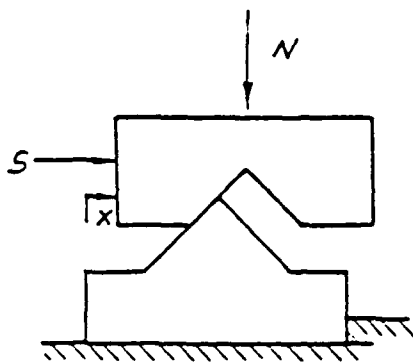
ϕ_s = friction angle for sliding between two plane surfaces of identical material

i = inclination of the asperity

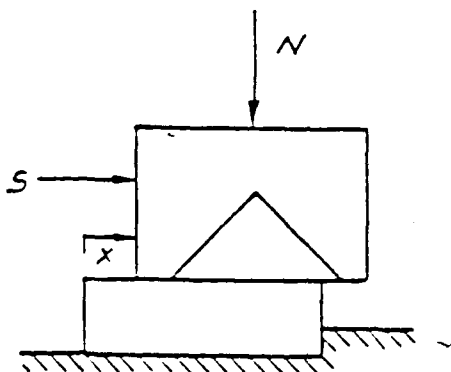
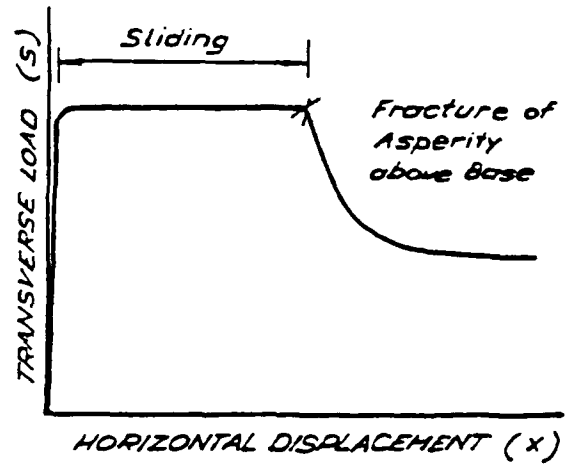
As the two asperities displace with respect to each other, a point is reached at which the stresses in the asperity will reach the strength, and the asperity will shear off at this level. If the normal force is increased, a stage is reached at which the asperities will shear at the base without any dilatancy.



a) INITIAL STATE



b) DILATANCY



c) SHEARING AT BASE

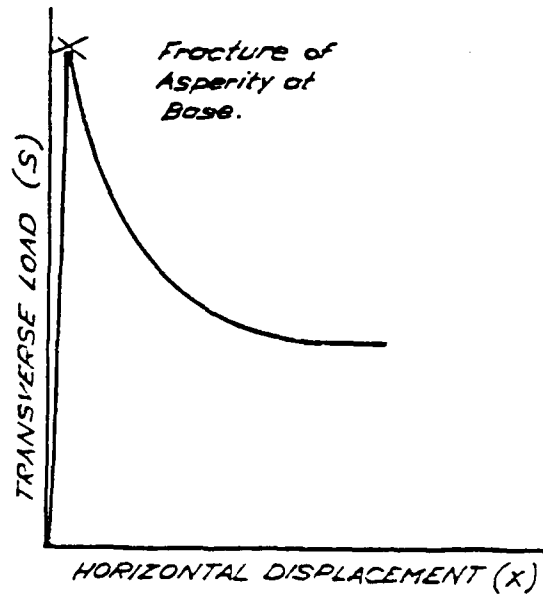


Fig. 4. Dilatancy and shearing of asperities. The mechanisms and corresponding load-displacement. From Einstein et al (1970).

For this stage, the relation between the stress and normal force is

$$S = K + N \tan \phi_r$$

where ϕ_r is the residual friction angle of the sheared material and K is a constant equal to the intersection with the shear force axis of the strength line used to approximate the S-N curve at high normal forces, as shown in Fig. 5. The various force displacement relations possible are shown in Fig. 4. In practice, the Mohr envelope will not be bilinear as shown in Fig. 5, but will be curved as shown in Fig. 6. This is because the asperities have different lengths and shapes, and consequently, the transition from dilatant to shear behavior is not sudden as implied by Fig. 5, but gradual, as shown in Fig. 6.

The Mohr envelope for the entire range of shearing is shown in Fig. 7. The two basic mechanisms governing the shear force -normal force relation, namely, sliding on existing or newly created shear surfaces and interlocking of asperities, result in the following general behavior. 1)dilatancy and subsequent shearing of asperities above their base - the initial curved section 2)shearing of asperities at their base and sliding along base - straight section 3)sliding along the sheared asperity base with plastic flow at the contact points leading toward complete contact - final curved and eventually horizontal section. Centrifuge modelling of a jointed rock requires that this behavior be scaled. If, the scaling relationships for each of the two basic mechanisms - sliding and interlocking are satisfied, then the shearing behavior of the joint will be correctly scaled.

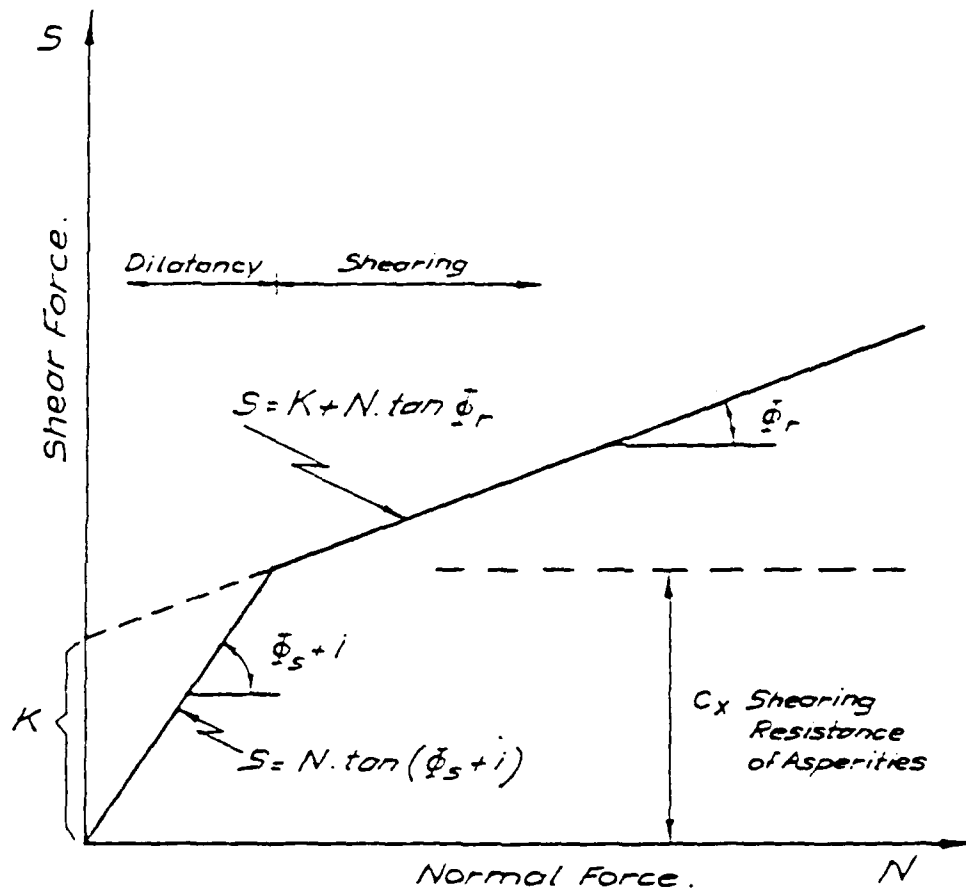


Fig. 5. Dilatancy and shearing of asperities. The characteristic Mohr envelope. From Einstein et al (1970).

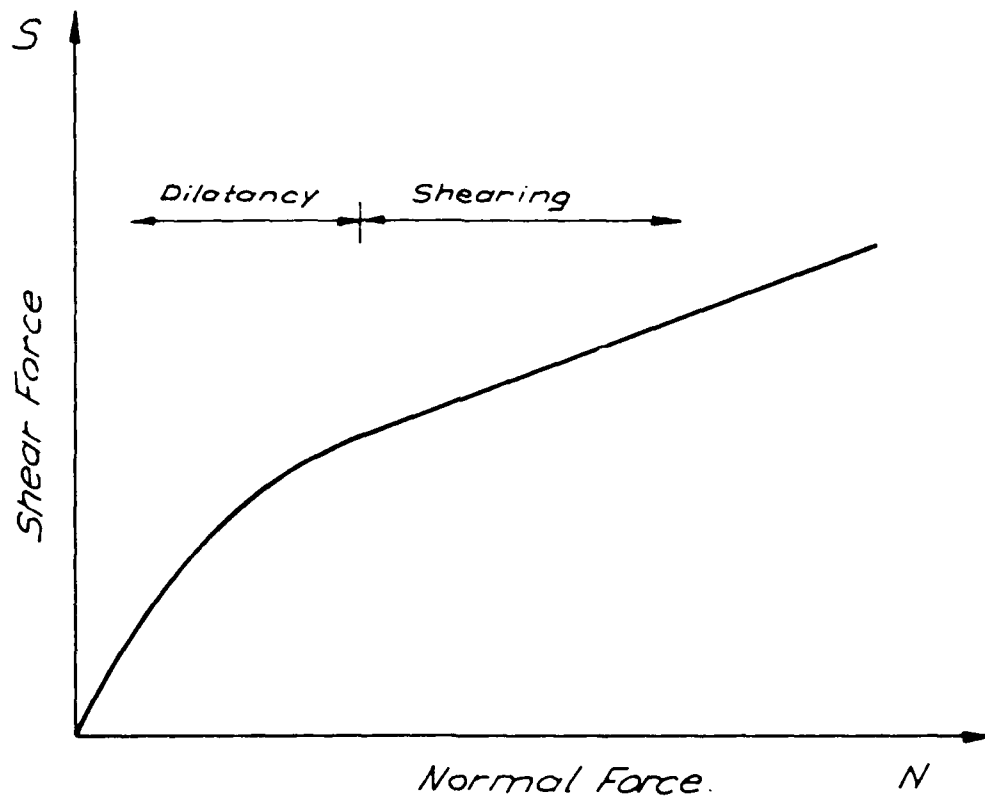


Fig. 6. Friction on surfaces with random asperities. Characteristic Mohr envelope. From Einstein et al (1970).

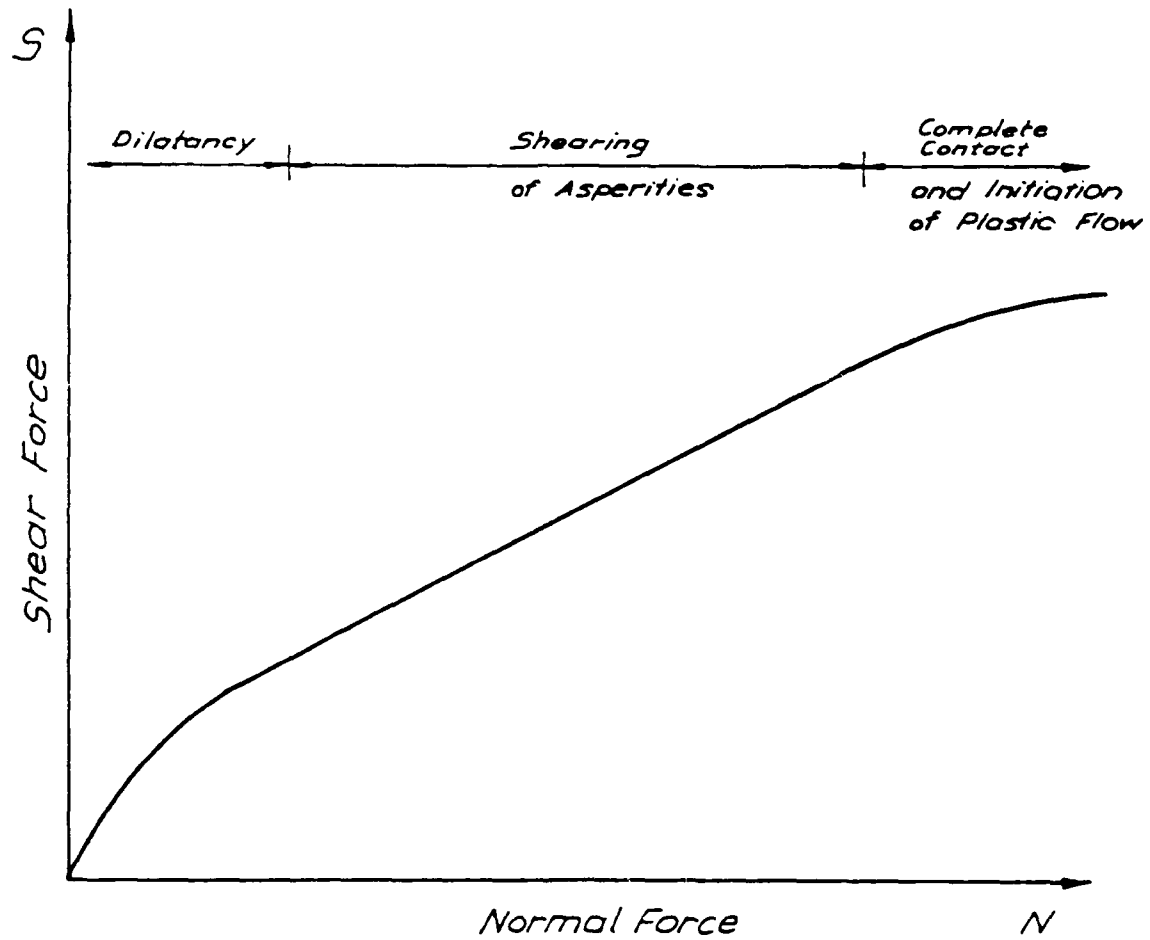


Fig. 7. Mohr envelope for the entire range of shearing.
From Einstein et al (1970).

1.3.2 Scaling relations for joint shearing

In this section, the scaling relationships for the two basic mechanisms - sliding and interlocking of the asperities will be determined.

Sliding between asperities was explained on the basis of the Terzaghi-Bowden-Tabor and Byerlee's theories for frictional sliding. The former requires that

$$\mu_m = \mu_p \quad (18)$$

while Byerlee's theory* requires that

$$\left(\frac{\sigma_t}{\sigma_c} \right)_m = \left(\frac{\sigma_t}{\sigma_c} \right)_p \quad (19)$$

in order that there be similitude. Byerlee's theory also requires that the geometry of the asperities be scaled. Geometric scaling is considered below when developing scaling relations for interlocking of the asperities.

Interlocking of asperities results in the shearing of asperities at or above their base. Shearing of asperities at their base occurs before any dilatancy, and sliding, on the newly created shear surface, then becomes the predominant mechanism. Shearing above the base is governed by the displacement and the geometry of the asperities, in addition to the material properties. The necessary scaling relationships for a single asperity, for shearing above the base, can be obtained using dimensional analysis as follows:

*

Byerlee (1967) based his theory on linear elasticity. For the materials involved and the range of stresses of the asperities, it is doubtful if behavior is linear elastic.

Consider the idealized interlocked asperity shown in Fig. 8. The independent variables that control the shear force - normal force relation are

L = the length of the asperity

B = the breadth of the asperity

H = the height of the asperity

ΔL = the dilatant movement in the vertical direction, up to fracture

M_N = the mass that results in the normal force acting on the asperity

g = the gravity that causes M_N to exert the normal force.

As explained in the accompanying report [Joseph et al (1987)], the dimensional matrix can be set up as

	k_1	k_2	k_3	k_4	k_5	k_6	k_7
	ΔL	L	H	g	B	M_N	τ
M	0	0	0	0	0	1	1
L	1	1	1	1	1	0	-1
T	0	0	0	-2	0	0	2

which is a matrix with rank $r = 3$. Consequently, the number of independent dimensionless products that can be obtained are $n - r = 7 - 3 = 4$.

By using the standard procedure of dimensional analysis, the following matrix can be obtained.

	ΔL	L	H	g	B	M_N	τ
Π_1	1	0	0	0	-1	0	0
Π_2	0	1	0	0	-1	0	0
Π_3	0	0	1	0	-1	0	0
Π_4	0	0	0	1	-2	1	-1

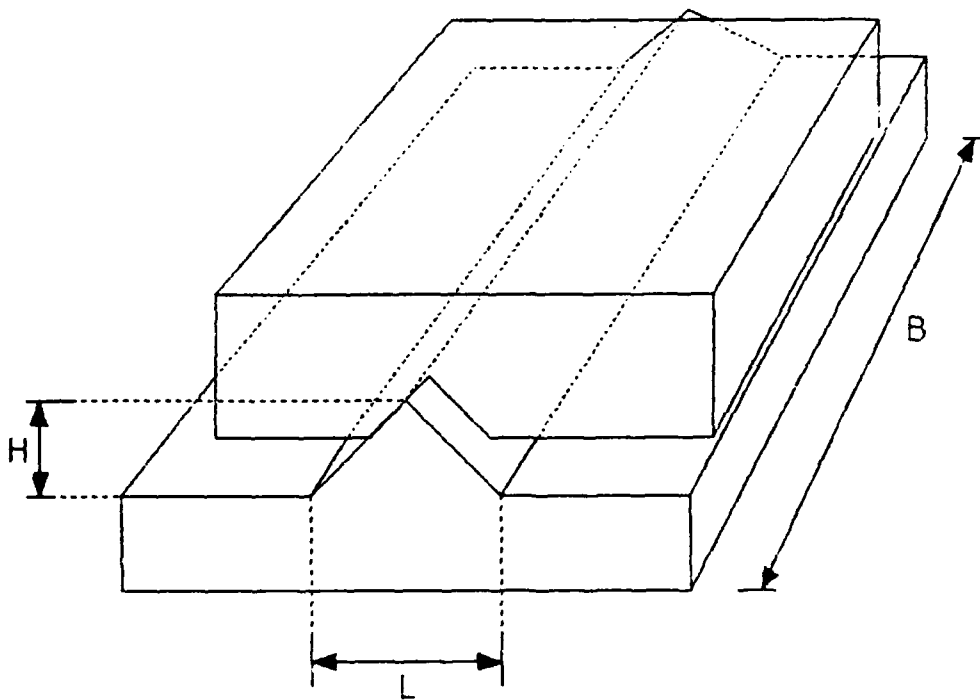


Fig. 8. Idealized asperity.

From this matrix the dimensionless Π terms can be written as

$$\frac{\Delta L}{B}, \quad \frac{L}{B}, \quad \frac{H}{B}, \quad \frac{g M_N}{B^2 \tau}$$

By suitably multiplying the above terms, all the independent variables can be combined in a single dimensionless product as

$$\frac{\Delta L}{B} \cdot \frac{B}{L} \cdot \frac{B}{H} \cdot \frac{g M_N}{B^2 \tau} = \frac{\Delta L}{L B H} \cdot \frac{M_N}{\tau} \cdot g$$

Hence, for similitude between model and prototype,

$$\left[\frac{\Delta L}{L B H} \cdot \frac{M_N}{\tau} \cdot g \right]_m = \left[\frac{\Delta L}{L B H} \cdot \frac{M_N}{\tau} \cdot g \right]_p$$

or

$$\frac{\Delta L_m}{\Delta L_p} = \frac{L_m}{L_p} \cdot \frac{B_m}{B_p} \cdot \frac{H_m}{H_p} \cdot \frac{M_{Np}}{M_{Nm}} \cdot \frac{\tau_m}{\tau_p} \cdot \frac{g_p}{g_m} \quad (20)$$

In equation (20), the normal force acting on the asperity i.e. F_N has been expressed in terms of the mass M_N and the acceleration in terms of 'g'. This renders the equation suitable for use in an elevated g field such as in a centrifuge. However, by using the fact that

$$M_{Np} \cdot g_p = F_{Np}$$

and

$$M_{Nm} \cdot g_m = F_{Nm}$$

Equation (20) can be rewritten as

$$\frac{\Delta L_m}{\Delta L_p} = \left(\frac{L_m}{L_p} \frac{B_m}{B_p} \frac{H_m}{H_p} \frac{\tau_m}{\tau_p} \frac{F_{Np}}{F_{Nm}} \right) \quad (20a)$$

which means that at 1g, by changing the magnitude of the mass resting on the asperity, one can alter F_N . In other words, Equation (20a) is valid, independent of the gravitational field in which the model or prototype is placed.

On examining Equation (20a), it is seen that there are four factors that are scaled. These are 1) the displacements at failure in model and prototype, namely $\Delta L_m/\Delta L_p$; 2) the asperity geometry in the model and prototype, namely, $(L_m H_m B_m)/(L_p H_p B_p)$, 3) the shear strength of the asperity material in the model and prototype, namely τ_m/τ_p and 4) the normal force on the asperity in the model and prototype, namely F_{Np}/F_{Nm} . The ratio of the displacement at failure, namely $\Delta L_m/\Delta L_p$ as expressed in Equation (20a) is dependent on the scales at which the remaining three factors, namely, the asperity geometry, the asperity strength and the normal force on the asperity are scaled. For the sake of generality, it can be assumed that they each have different scale factors. Hence, let the geometry of the asperity be scaled at S and the shear strength as $\frac{\tau_m}{\tau_p}$. The normal force on the asperity can be scaled either in terms of geometry, the mass, or in terms of the gravitational field acting on the model.

To illustrate the above statement, the scaling the of the normal force is considered in more detail in this paragraph. As mentioned, there are three ways in which the scaling can be done. The first is by scaling the geometry of the entire body resting on the asperity say at $S = N$ in which case,

$$\frac{M_{Np}}{M_{Nm}} = N^3$$

The second possibility is to scale the mass alone at N in which case

$$\frac{M_{Np}}{M_{Nm}} = N$$

The third possibility is to use any mass, and, to scale the gravitational field in which case.

$$\frac{F_{Np}}{F_{Nm}} = \frac{M_{Np} g_p}{M_{Nm} g_m}$$

From this equation is is seen that if $M_{Np} = N M_{Nm}$ and $g_p = \frac{1}{N} g_m$,

then $F_{Np} = F_{Nm}$.

To restate again, the most general case is expressed by Equation (20), with the asperities scaling at say S , the shear strengths and masses as any value and the gravity at N . Based on this, equation (20) can be written as

$$\frac{\Delta L_m}{\Delta L_p} = \frac{1}{S^3} \frac{\tau_m}{\tau_p} \frac{M_{Np}}{M_{Nm}} \cdot \frac{g_p}{g_m} \quad (21)$$

Examination of this equation shows that there are various possibilities available for scaling.

Case 1) In this case, the asperity geometry is scaled at N, (i.e., $S = N$) the geometry of the mass resting on the asperities is scaled at N and the model is spun at N_g . For these conditions equation 21 reduces to

$$\frac{\Delta L_m}{\Delta L_p} = \frac{1}{N^3} \frac{\tau_m}{\tau_p} N^3 \frac{1}{N}$$

or

$$\frac{\Delta L_m}{\Delta L_p} = \frac{1}{N} \frac{\tau_m}{\tau_p} \quad (22)$$

Case 2a) In this case, let the asperity geometry scale at S, the geometry of the mass resting on top of the asperity scale at N, and let the model be spun at N_g on a centrifuge. For these conditions, equation 21 reduces to

$$\frac{\Delta L_m}{\Delta L_p} = \frac{1}{S^3} \frac{\tau_m}{\tau_p} N^3 \frac{1}{N}$$

$$\text{i.e.} \quad \frac{\Delta L_m}{\Delta L_p} = \frac{N^2}{S^3} \frac{\tau_m}{\tau_p} \quad (23)$$

It can be seen that for $S = N$ (case 1) Equation 23 reduces to Equation 22.

Case 2b) In this case, rather than scale the geometry of the mass resting on the asperity at N, let the mass itself be scaled at N, i.e., let $\frac{M_{NP}}{M_{Nm}} = N$.

In this case, equation 21 reduces to

$$\frac{\Delta L_m}{\Delta L_p} = \frac{1}{S^3} \frac{\tau_m}{\tau_p} N \frac{1}{N}$$

or

$$\frac{\Delta L_m}{\Delta L_p} = \frac{1}{S^3} \frac{\tau_m}{\tau_p} \quad (24)$$

From these cases it is clear that the general relationship is given by Equation (21), which in turn is equation (20) expressed in terms of the model to prototype ratios.

Let Equation (21) be written for a model (say model 1) of a prototype

$$\frac{\Delta L_{m1}}{\Delta L_p} = \frac{1}{S_1^3} \frac{\tau_{m1}}{\tau_p} \frac{M_{Np}}{M_{Nm1}} \frac{g_p}{g_{m1}} \quad (25)$$

Let another model (say model 2) be used to model the same prototype, but at a different scale. Equation 21, for this case becomes

$$\frac{\Delta L_{m2}}{\Delta L_p} = \frac{1}{S_2^3} \frac{\tau_{m2}}{\tau_p} \frac{M_{Np}}{M_{Nm2}} \frac{g_p}{g_{m2}} \quad (26)$$

Dividing Equation (25) by Equation (26), we get

$$\frac{\Delta L_{m1}}{\Delta L_{m2}} = \frac{S_2^3}{S_1^3} \frac{\tau_{m1}}{\tau_{m2}} \frac{M_{Nm2}}{M_{Nm1}} \frac{g_{m2}}{g_{m1}}$$

By suitably separating the terms in this equation we can write

$$\frac{\Delta L_{m1}}{\tau_{m1}} \frac{S_1^3}{M_{Nm1}} \frac{g_{m1}}{g_{m1}} = \frac{\Delta L_{m2}}{\tau_{m2}} \frac{S_2^3}{M_{Nm2}} \frac{g_{m2}}{g_{m2}}$$

In other words, for any model,

$$\frac{\Delta L_m}{\tau_m} \frac{S_m^3}{M_{Nm}} \frac{g_m}{g_m} = \text{a constant} = \frac{\Delta L_p}{\tau_p} \frac{M_{Np}}{M_{Np}} \frac{g_p}{g_p}$$

As can be seen, when testing models at 1g, this equation reduces to

$$\frac{\Delta L_m S_m^3 M_{Nm}}{\tau_m} = \frac{\Delta L_p M_{Np}}{\tau_p} = \text{a constant} \quad (27)$$

This means that Equation 20 is valid if the relation given by Equation (27) is true. This relationship can be verified by shear tests at 1g.

In Equation 20, by replacing the term $M_{Np} g_p$ by W_p (the prototype weight) and $M_{Nm} g_m$ by W_m , the model weight, it becomes clear that the relation can be verified at 1g, i.e., to verify this equation, it is not necessary to use a centrifuge.

It is worth studying Equation 20 as it applies to centrifuge testing. Let the prototype to be modelled consist of a joint within a rock mass. There are several ways in which this joint can be scaled.

Possibility 1. Let the mass of the model blocks in the rock mass be $\frac{1}{N}$ those of the corresponding prototype blocks, and let the model asperities and model material be the same as those of the prototype i.e. $S = 1$ and $\tau_m = \tau_p$. Let the model be spun at Ng in order to obtain the same surface tractions. For these conditions, Equation 20 reduces to

$$\frac{\Delta L_m}{\Delta L_p} = 1^3 \cdot N \cdot 1 \cdot \frac{1}{N} = 1$$

i.e. as expected, when the tractions on the surface of the model joint are the same as those on the prototype, and if, the geometry and material properties of the model are the same as those of the prototype, then the movements too will be the same.

Possibility 2. Let a model material be used for which $\tau_m = \tau_p$, but S is not 1 as in the previous case, but say N . Let the geometry of the material above the joint be scaled at $1/N$, and to get the same surface tractions, let the model be spun at Ng . In this case, Equation 20 reduces to

$$\frac{\Delta L_m}{\Delta L_p} = \frac{1}{N^3} \cdot 1 \cdot N^3 \cdot \frac{1}{N}$$

This means that $\Delta L_m = \frac{1}{N} \Delta L_p$ or that

$$\epsilon_m = \frac{\Delta L_m}{L_m} = \frac{\frac{1}{N} \Delta L_p}{\frac{1}{N} L_p} = \epsilon_p$$

i.e. if the asperity geometry is scaled at $1/N$ and if the mass M_N is scaled at $\frac{1}{N^3}$, then imposing the same stresses in the model as in the prototype will result in the model having the same strains as the prototype.

Possibility 3. Suppose a jointed work mass of several blocks is to be modeled using model blocks that are geometrically scaled at $\frac{1}{N}$, but whose asperities are not scaled, i.e. $S = 1$. Then, if it is required that the model strains (strains being defined as $\Delta L/L$ where L is a dimension of the asperity) be equal in the model and the prototype for equal stresses, it is necessary that $\Delta L_m = \Delta L_p$. Substituting in equation 20,

$$\frac{\Delta L_m}{\Delta L_p} = 1 = \frac{1}{1} \cdot \frac{\tau_m}{\tau_p} \cdot N^3 \cdot \frac{1}{N}$$

$$\text{or } \tau_m = \frac{1}{N^2} \tau_p$$

i.e. if the rock blocks are geometrically scaled at $\frac{1}{N}$, with the asperities unscaled ($S = 1$), then in order that strains and displacements be the same at

equal stresses, it is required that

$$\tau_m = \frac{1}{N^2} \tau_p$$

Possibility 2 suggests that if a rock mass is modelled by blocks of the same rock and geometrically scaled (both block and asperity) at $\frac{1}{N}$, then model displacements will be $\frac{1}{N}$ prototype displacements and model strains will equal prototype strains, both at the same stresses. Possibility 3 suggests that if the rock blocks are scaled at $\frac{1}{N}$ with the asperities unscaled and if the model material is N^2 times weaker than the prototype material, then the strains and the displacements in the model and prototype will be equal, at equal stresses.

In conclusion it must be noted that

$$\frac{\Delta L_m S^3 M_{Nm} g_m}{\tau_m} \text{ normalized with respect to } L_p B_p H_p \text{ is}$$

$$\frac{\Delta L_m M_{Nm} g_m}{L_m B_m H_m \tau_m} \text{ which is}$$

a dimensionless product. By reproducing the prototype phenomenon in the model, we require that the dimensionless product that defines this phenomenon be the same in the model. This requires that for all models, the dimensionless product be equal to its prototype value or

$$\frac{\Delta L_m M_{Nm} g_m}{L_m B_m H_m \tau_m} = \text{a constant} = \frac{\Delta L_p M_{Np}}{L_p B_p H_p \tau_p} \quad (\text{with } g_p = 1)$$

or that

$$\frac{\Delta L_m S^3 M_{Nm} g_m}{\tau_m} = \text{a constant} = \frac{\Delta L_p M_{Np}}{\tau_p}$$

where S is the asperity geometry scale.

1.4 Conclusion

In this chapter, the various scaling relations applicable to an intact rock and a joint were determined. It was found that changing the gravitational field of the model by spinning it in a centrifuge, resulted in considerable flexibility of modelling as compared with the case of modelling at 1g. Once the modelling of intact rock and a joint has been successfully accomplished, it will be possible to model a jointed rock mass.

Chapter 2. Proposed Rock Mechanics Research Using the Centrifuge

2.1 Introduction

In the accompanying report, details were provided about the principles of centrifuge testing and a review made of centrifuge work done in rock mechanics. It was seen that initially (in the fifties and early sixties) the centrifuge was used more for studying problems in rock, than soils. Gradually the situation changed until in the seventies, almost all the work was done in soil mechanics. This was because soils are more amenable to testing at relatively low g levels. In the last few decades, considerable theoretical work has been done in rock mechanics. The centrifuge can be used to verify the various theories developed. Where no theoretical models exist, the centrifuge can be used to gain more insight into the problem. Scaling relations for intact rock and for a joint were developed in the previous chapter of this report. This chapter studies areas where the centrifuge can be of use.

2.2 Proposed research

The proposed research deals with basic issues in rock mechanics, such as shearing along a joint, then leading to sliding of a block on a joint and to the behavior of a wedge in various stress fields, and finally, the behavior of slopes, arching in tunnels and other problems. The general objectives are to conduct experiments on behavior which is difficult to observe in nature or on behavior for which recent theoretical models are based on simplifying assumptions, or both. For some phenomena, nothing direct is known about the

failure mechanism and only the evidence available after failure is used to hypothesize pre and post failure behavior. The proposed research will be grouped under the following sub-headings. 1) Conditions where stress distribution and or gravity play a role and not involving the flow of water or dynamic events 2) conditions involving water and 3) rock dynamics. These areas will be discussed below.

2.2.1 Conditions where stress distribution and/or gravity play a role

There are several basic problems that can be studied using the centrifuge. For some of these, theories and models of various degrees of sophistication exist, while for others not enough is known to formulate a model. Centrifuge tests can be used either to validate the existing theories or to gain more insight into the failure mechanisms. The actual failure is in general difficult to observe in the field, whereas a controlled failure in the centrifuge can be observed and recorded. Once these basic issues are better resolved, then their interaction with water and dynamics can be studied. Consequently, in this report, emphasis will be placed on static or quasi-static problems involving no water.

A basic problem is the sliding of a block on an inclined plane. The commonly used limit equilibrium analysis cannot address stress distribution effects, and the actual contact stresses may deviate significantly from these assumed. Further, in the usual analysis, the failure mechanism assumed is based on simplifying assumptions regarding initiation of movement, the factors that affect the movement, whether failure occurs with the block moving in translation or rotation, if it topples or if combined failure modes (translation and rotation) occur. By modelling the process on the centrifuge,

important information regarding the entire failure mechanism i.e. pre-failure, failure and post-failure behavior can be obtained. By varying the surface roughness, the influence of the surface can be studied. The effect of various forces on block movement can also be investigated. An idea of the stress distributions across the face of the block can be obtained by suitable gageing and so, a measure of the effect of stress distribution on movement can be obtained. The suitability of different methods of analysis can be examined by duplicating their implicit assumptions in the tests and comparing them with the results. The methods of analysis that will be studied are the usual limit equilibrium analyses and also the method of artificial supports [Chan and Einstein (1981)] as well as some numerical approaches.

An extension of this problem is the case of a single block or wedge on multiple planes. Here too, the stress distribution at the base of the wedge is not known. A number of analytical approaches show the importance of stress distribution in the planes on stability [Chan and Einstein (1981)]. However, the approaches use different basic assumptions. For this case, even less is known about movement of the block and stress changes at the interface, than for the case of a block as a single plane. By measuring displacement and, stresses under controlled conditions, questions of interest such as when does movement take place on a single plane, or on both planes, when does rotation occur and how do these movements compare with predictions made from analytical models, can be answered. The effects of in-situ stresses, external forces, surface roughness and joint stiffness can also be studied. As in the single plane case, here too, it is of interest to specifically model particular

analytical assumptions and compare the results of the tests with those predicted by the analyses.

The test runs discussed above will provide information that will be useful in every area of rock mechanics and underground construction in rock, where rock wedges and blocks are likely to be encountered, and particularly where wedges and blocks interact. The interaction of several rock blocks prior to and during failure is not well understood. During instability, any combination of rotation and translation of the individual blocks may occur so much so that sometimes this may lead to dilatancy, which will prevent failure. By observing such behavior in the centrifuge, additional information will be obtained, leading ultimately to the development of an analytical model. An extension of studies on block interaction are studies of arching of rock blocks, which is of interest in various underground construction problems such as tunnels, caverns, etc. The load deformation behavior of tunnels can be studied with arching tests. There is a dispute about the load deformation behavior of the supports. Everybody agrees that the so called ground reaction curve shows a decreasing load with increasing support displacement. At very large displacements, some authors claim [Steiner and Einstein (1980)] that the loosened material above the support results in an increase in load in the tunnel support. The combined effect of gravity and far field stresses is not understood and needs to be studied. Arching tests will also be useful for tunnels in soil since the same mechanism is operative there too. Also, three dimensional effects at or near the tunnel face can be investigated with such tests run in soil. More complex tunnel geometries such as intersections with larger openings, etc. can be studied in rock mass arching tests. Initially simple geometries will be used,

leading eventually to the study of more complex joint patterns. Ultimately, key block geometries can be investigated and compared with the results of corresponding analyses. Observations will be the deformation and loads on the supports which will be in the form of a trap door. Results from these tests will provide information on how rock blocks interact, and will be of use in the analysis of jointed rock slopes.

Rock block breaking is related to rock fall which will be discussed below.* Blocks impacting against each other or impacting against fixed rock surfaces can break up. The mechanism by which they break up and what block sizes and shapes result will effect the character of the entire failure and how the falling rock mass comes to rest. Here too, original information based on observation of blocks after they come to rest is not satisfactory. Blocks of various sizes will impact against each other and fall on fixed surfaces under the influence of gravity. Initially, video recordings of the disintegration will be made, and will lead to a better understanding of the process, and ultimately, to measuring the process. The variables involved will be block size, shape, the number of blocks, the height of fall, and the inclination of the fixed surface.

The rock breaking study is only a step towards investigation of rock fall, which is one of the least understood processes. Massive rock falls or rock avalanches have similarities with snow avalanches and slides of other particular media. Consequently, mechanisms of high pore pressures (liquid or gas) and of cyclic or dynamic mobility have been proposed to explain the movement of such avalanches. Again, in-situ observations are limited and

*Both rock block breaking and rock fall can also be considered as dynamic problems.

there is no unequivocal evidence for the rock fall mechanism. Rock fall involving a limited number of particles (including the falling of a single one) has been treated empirically, analytically and numerically, the latter involving the falling, bouncing and rolling of simple models of individual spheres, ellipsoids and a few other shapes. Centrifuge observations of the single particle mechanism (fall, jump, roll and break up) and of the multi-particle interaction process, with interaction between the particles, will clarify the issue and provide a basis for measurements and theoretical treatment.

Tests, run in the areas described above will provide new data, leading to the verification of existing theoretical models, the development of new models, or, an increase in an understanding of the phenomenon.

2.2.2 Conditions involving water

Once a jointed rock mass has been successfully modelled in the centrifuge, then problems involving the flow of water in jointed rock masses can be studied. A question of interest is whether water flows through a fractured rock mass in a manner similar to a pipe network. The idea that one does not have parallel plate flow but channeling can also be studied. Finally, the question of deformation-flow coupling can be studied, i.e. what is the effect of this coupling on channeling and on stability (stress distribution) and vice versa.

2.2.3 Conditions involving dynamics

Once basic testing has been successfully done, then dynamic effects can be studied. Problems of interest are the Newmark/Whitman block problem (a block on a slope that is subjected to base shaking), and blast cratering. The latter is to extend studies already done on soils to rock and in order to study damage due to explosions. Another topic of interest concerns the effects of shock waves on a jointed rock mass. All these problems can be conveniently and more realistically modelled on the centrifuge.

2.3 Problems involved with centrifuge tests of rock

There are a few basic problems that have to be investigated and solved. One such problem is that of the joint surface asperities. In Chapter 1 of this report, the criterion for joint similitude was established. This relationship will have to be verified by direct shear tests of different asperities. Once the intact rock and the joint have each been successfully scaled, then the jointed rock mass as a whole can be modelled. When it comes to including water and dynamics, then appropriate scaling relations will have to be derived, that satisfy the similitude conditions. At present however, the main problem is the correct scaling of the joint surface.

Chapter 3. The Testing Program

3.1 Introduction

This chapter proposes tests to investigate the areas of research described in Section 2.2.1. The surface roughness plays a role in all the areas, and so, the first aim is to study the surface roughness to see if asperity behavior scales as suggested by equation (20) in Chapter 1. Another basic objective is to be capable of obtaining some idea of the stresses on the surface of sliding or contact. Consequently, it is suggested that the first test series of the testing program be directed towards these two areas. The following section considers each of the areas of research suggested in Section 2.2.1 and proposes experiments to study these areas. The issues involved, the variables concerned, the methods of testing and the experimental problems likely to be faced will be discussed. Either natural or intact rock will be used, depending on the nature of the experiment.

3.2 The testing program

3.2.1 Scaling of asperities

The aim is to study if the shearing of asperities scales when the similitude requirements as suggested in Chapter 1 are satisfied. In order to best study this, an idealized asperity such as shown in Fig. 8 will be used. The variables involved are the geometry of the asperity, the material properties and the normal force acting on the asperity. Once the relationships developed have been verified for the idealized asperity, then a natural rock surface will be studied, and the scaling relationships for joint behavior developed for use in subsequent testing programs. The choice of material used to make the artificial rock will be based on research done by

Einstein et al (1973). A common problem for tests involving jointed rock is the scaling of both the intact rock and the joint surfaces. If the material strength of the intact rock is too high, then there will be no shearing off of asperities and the effect of dilatancy will be too high.

An extension of these tests is to study the effect of stress distribution on shearing behavior. For this, the orientation of the surface of sliding for the two blocks will be varied resulting in a change in the stress distribution of the surface of contact. The effect of the different contact stress distributions on the normal stress and shear stress versus displacement curves will be studied.

In both these series of tests, the measured variables will be the normal force, the shear force and the displacement of the top block relative to the bottom block.

3.2.2 Stresses on the sliding surface of a block

The ability to determine tractions on the surface of sliding will be of use in a number of proposed experiments. In experimental soil mechanics, there are several contact stress transducers, designed to measure the shear stresses and normal stresses at the surface. These, however, are designed for use at 1g. No device seems to exist on the market that is suitable for use at high g levels. Consequently, suitable strain gageing will be developed to determine the surface tractions.

3.2.3 Block on an inclined plane

These tests will involve a block sliding on a single plane. The issues of interest will be the failure mode, i.e. the type of movement before,

during, and after failure, and also, the stress distribution throughout the process. The variables involved are the slope angle, the surface roughness, the externally applied forces, the stress distribution and the geometry of the block. The quantities measured will be the displacements and the stresses (as in Section 3.2.2). Tests which model the simplified assumptions of various analyses (the limit equilibrium and method of artificial supports) will also be run to check the validity of these analyses. For running these tests it may be necessary to be able to change the slope angle in flight, in an accurate and controlled manner. This will require the construction of an inclined plane whose slope can be controlled hydraulically or mechanically. Both natural and artificial rock will be used in the experiments.

3.2.4 Single block or wedge on multiple planes

These tests are an extension of the previous tests. The issues of interest are the stress distribution during the entire sliding process, right from initiation, and the type of movement at the start of, during, and after failure. The variables are the same as in the previous case, with additional variables being the angle between the two planes and the stresses imposed by the two planes on the wedge. Comparisons will be made between experimental and theoretical results and tests will be run with the specific aim of modelling the assumptions of available theories so as to check their validity. Here too, both natural and artificial rock will be used. In this case, measuring the stresses on the sliding surfaces will not be as straightforward as suggested in Section 3.2.2.

3.2.5 Multi-block failures

The aim is to study the interaction of multiple blocks on a plane and to determine what criteria govern the failure mode (e.g. rotation vs. translation). Dilatancy too may occur under certain conditions, and an attempt will be made to determine what these conditions are. The interaction effects will be governed by the geometry of the individual blocks, the arrangements of the blocks, the surface roughness of the blocks, the strength of the asperities and the externally applied stresses. A series of experiments will be run to see if the interaction of the blocks scales with size and, to study the effects of all variables listed on the overall behavior.

The interaction of a group of blocks will also be studied using a trap door arching experiment as shown in Fig. 9. The aim of this test is to see whether the behavior of a jointed rock mass can be scaled, and to gain insight into arching of jointed rock. This can be determined by studying the force-settlement relationship for the rock mass and seeing if it scales from one size of experiment to another. After each experiment, the rock mass will be carefully taken apart to observe the amount and the location of sliding between the blocks. Similar experiments have been used successfully to study the behavior of soils lying above a yielding trap door. The variables whose influence can be studied in these experiment are the effect of two-dimensional versus three-dimensional geometry (a long strip door vs. a square door), the thickness of the rock mass relative to the trap door width, the joint geometry, the model material and the surface characteristics. The dimensions of the blocks to be used depend on the model material and the scales at which the proposed tests will be run.

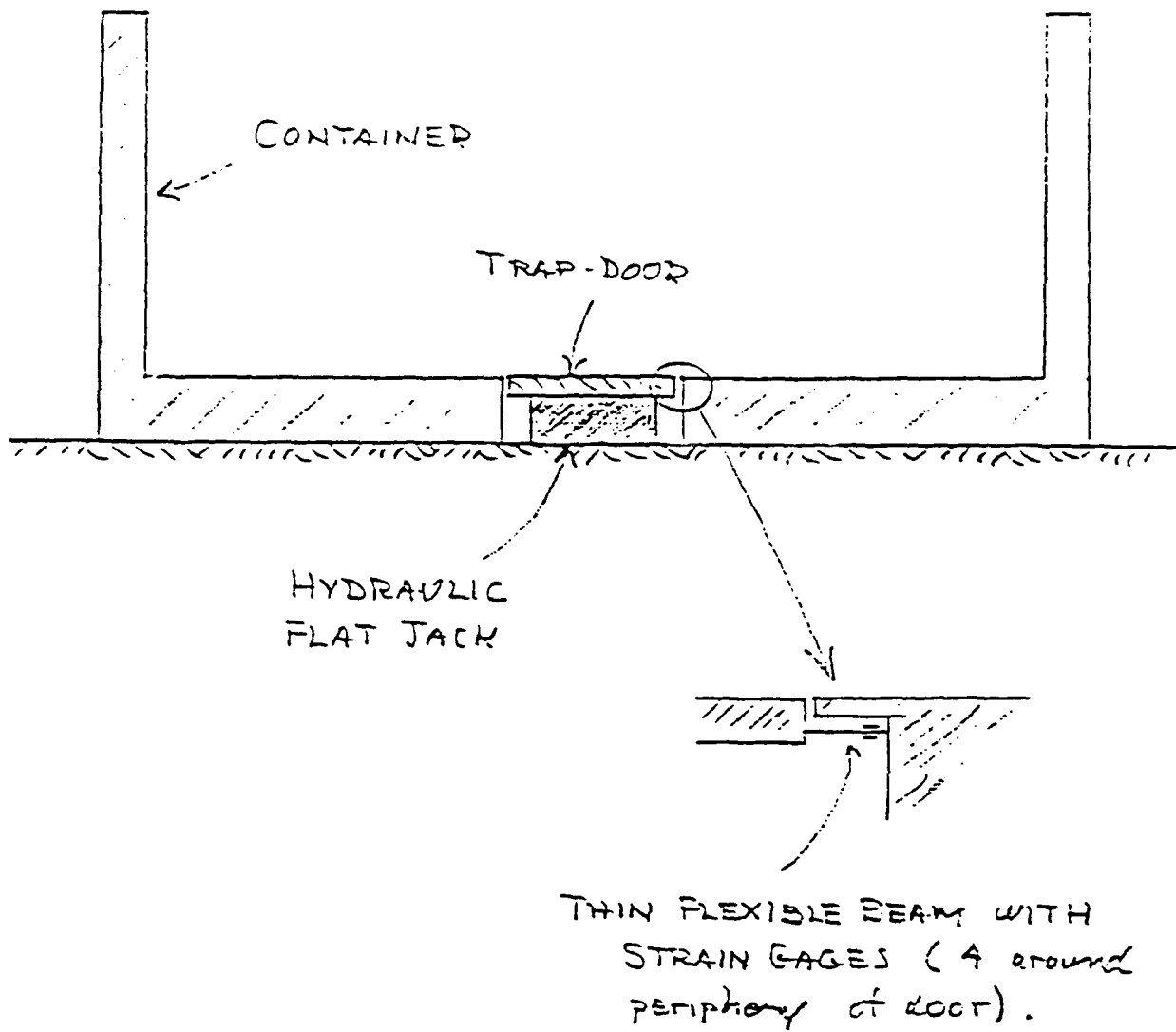


Fig. 9. Arrangement for trap-door experiment.

The experiments described above can be extended to study tunnels in jointed rock masses. Of interest will be the modelling of the three dimensional geometry near the tunnel face, leading eventually to the study of tunnels intersecting other underground openings of various shapes. Initially, however, relatively simple geometries will be used, involving the study of block geometries and also support behavior. Here too, observations will be made on the deformations and loads.

3.2.6 Break up Tests

The aim of these tests is to study the mechanism by which rocks impacting against one another or against a fixed surface break up. Of interest will be the geometry of the resulting pieces and their displacement behavior. The variables will be the geometry (size and shape) of the block, the number of blocks, the height of fall and the inclination of the surface of impact. The impacting blocks have to be unrestrained, causing problems of instrumentation. Consequently, only visual observations and video recordings will be initially made. During these tests, an effort will be made to develop new techniques to make measurements on individual block behavior. Based on these tests, a program of tests to study one of the least understood problems in rock mechanics - rock falls and avalanches - will be developed.

3.2.7 Rock Fall and Avalanche Tests

These tests are an extension of the tests described above. Rock falls and avalanches are not well understood and the primary aim of these tests will be to obtain a better understanding of the process through visual observations, at the same time recording it on video for further analysis as required. On the basis of tests as described in Section 3.2.6, more detailed measuring

techniques will be determined. Avalanche tests are more complicated than rock fall tests since they involve pore pressures. Simulating pore pressures will first require the development of suitable scaling relations to determine what the similitude requirements of the model pore fluid will be. The dynamic mobility effect also plays a role and will have to be treated separately from the pore pressure. It is also not known at present how one can judge if one or the other of the two mechanisms takes place and how one would measure the pore pressures. Suitable testing techniques that can handle these problems will have to be developed.

3.3 Conclusion

The tests discussed above have been presented in order of increasing complexity, with almost every series depending on the previous test series. Once intact rock and joint surfaces have been modelled, then one can proceed to model the jointed rock mass. Based on accumulated experience, more complex problems can be tackled, ultimately leading to the study of problems involving fluids and dynamics. Almost no centrifuge testing has been done so far with jointed rock and consequently much can be learned from such tests.

List of References

- Bowden, F.P. and Tabor, D. (1967), "Friction and Lubrication of Solids," Methuen, London, pp. 166.
- Byerlee, J.D. (1967), "Frictional Characteristics of Granite under High Confining Pressure," Journal of Geophysical Research, Vol. 72, No. 14, July, pp. 3639-3648.
- Chan, H.C. and Einstein, H.H. (1981), "Approach to Complete Limit Equilibrium Analysis for Rock Wedges - The Method of 'Artificial Supports' ", Rock Mechanics, Vol. 14, No. 2, pp. 59-86.
- Einstein, H.E, Bruhn, R.W., and Hirschfield, R.C. (1970), "Mechanics of Jointed Rock," Report R70-62 to the U.S. Department of Transportation, August, pp. 115.
- Einstein, H.E. and Hirschfield, R.W. (1973), "Model Studies on Mechanics of Jointed Rock," Journal of Soil Mechanics and Foundation Engineering, ASCE, Vol. 99, No. SM3, March, pp. 229-248.
- Esser, R.H.K. (1962), "A Model Study of the Application of Roof Bolts under Unsymmetric Loading Conditions," M.S. Thesis, University of Missouri School of Mines.
- Hoek, E. (1965), "The Design of a Centrifuge for the Simulation of Gravitational Force Fields in Mine Models," Journal of the South African Institute of Mining and Metallurgy, Vol. 65, No. 9, pp. 455-487.
- Haycocks, C. (1962), "Mechanics of a Voussoir Arch," M.S. Thesis, University of Missouri School of Mines.
- Joseph, P.G.; Einstein, H.H. and Whitman, R.V., (1987), "A Literature Review of Geotechnical Centrifuge Modeling with Particular Emphasis on Rock Modeling," Report to the Air Force Engineers and Service Center, Tyndall Air Force Base, Florida. Contract No. DACE-86-D-0013.
- Oudenhoven, M.S. (1962), "A Model Study of the Behavior of Elastic Liners in Shallow Underground Openings," M.S. Thesis, University of Missouri School of Mines.
- Steiner, W. and Einstein, H.H. (1980), "Improved Design of Tunnel Supports: Volume 1 - Empirical Methods in Rock Tunneling - Review and Recommendations," Report No. UMTA-MA-06-0100-80-8, U.S. Department of Transportation, Urban Mass Transportation Administration.
- Terzaghi, C. (1920), "New Facts About Surface Friction," The Physical Review, N.S. Vol. XVI, No. 1, pp. 54-61; Reprinted in From Theory to Practice in Soil Mechanics, pp. 165-172, Wiley, New York, 1961.